

Hall and Gyro-Viscosity Effects on the Rayleigh-Taylor Instability in a 2D Rectangular Slab

Ryosuke GOTO¹⁾, Hideaki MIURA^{1,2)}, Atsushi ITO^{1,2)}, Masahiko SATO²⁾ and Tomoharu HATORI¹⁾

¹⁾*The Graduate University for Advanced Studies, 322-6 Oroshi-cho, Toki, Gifu 509-5292, Japan*

²⁾*National Institute for Fusion Science, 322-6 Oroshi-cho, Toki, Gifu 509-5292, Japan*

(Received 5 August 2013 / Accepted 18 January 2014)

Effects of the Hall term and the gyro-viscosity on the Rayleigh-Taylor instability in a 2D rectangular slab are studied numerically. Nonlinear magneto-hydrodynamic (MHD) simulations with these effects reveal that the combination of the Hall term and the gyro-viscosity causes the lower growth rates and the lower saturation level of unstable modes relative those in the single-fluid MHD case, while neither the gyro-viscosity nor the Hall term shows a strong stabilization effect only by itself. It is also shown that the mixing width of the density field can grow as large as that in the single-fluid MHD case, even though the saturation level of the kinetic energy is lowered and the detailed density profile becomes sharper. These numerical results suggest that the extension of the MHD equations can bring about a growth of unstable modes in a lower level, although it does not necessarily mean a weaker impact of the instability to the equilibrium.

© 2014 The Japan Society of Plasma Science and Nuclear Fusion Research

Keywords: extended MHD, Hall effect, gyro-viscosity, Rayleigh-Taylor instability

DOI: 10.1585/pfr.9.1403076

1. Introduction

Dynamical growth of magneto-hydrodynamic (MHD) instability has been studied extensively by means of numerical simulations.

A special interest of nonlinear numerical simulations is on growth and saturation of the ballooning/interchange instability since behaviors of these instabilities over a short-length-scale can play a significant role in various aspects of torus plasma dynamics, such as high-beta achievements in the Large Helical Device (LHD) [1] and the edge localized modes (ELMs) in tokamaks [2, 3]. There have been some numerical works which report a nonlinear saturation of the ballooning/interchange modes without a large reduction of the peak pressure [4–6]. In these simulations, large values of the dissipative coefficients, such as the viscosity and the heat conductivity in the direction perpendicular to the magnetic field lines, are adopted, although plasma dynamics is considered to be almost collision-less. However, full three-dimensional (3D) MHD simulations of LHD with relatively small dissipative coefficients show that the growth of the ballooning modes can bring about a reduction of the peak pressure of more than 20% before the saturation [7], even though the corresponding experiments show a mild behavior without such a large reduction of the core pressure in spite of its unstable profile [8]. In order to explain the disagreement between numerical simulations with small dissipative coefficients over experiments, an additional mechanism to suppress the growth of the ballooning/interchange modes is required.

Some mechanisms to suppress the growth of the ballooning/interchange modes have been proposed in the framework of the single-fluid MHD equations [4, 5]. Since simulations of a full set of 3D compressible and nonlinear MHD equations including all these mechanisms have shown some disagreements with the experiments [7], it suggests that the mechanisms proposed earlier in the framework of the single-fluid MHD are insufficient to suppress unstable modes, and it may be appropriate to find a new mechanism not in the single-fluid MHD model but outside of it. One possibility is short-length-scale effects such as the finite Larmor radius (FLR) effects and the Hall term (or the two-fluid terms), which do not appear in the MHD equations. These effects can not be neglected in unstable short-length-scale modes, and can influence nonlinear saturation even when the dissipative coefficients are fairly small.

A set of fluid equations with short-length-scale effects has been derived by Braginskii in the collisional context [9]. Though Braginskii's approach is quite rigorous, the equations are too dissipative for a torus plasma. In stead of the rigorous Braginskii equations, slightly modified ones, sometimes referred to as extended MHD equations [10] can be used. A frequently-used extended MHD model is similar to the Braginskii's equation: Braginskii's ion stress tensor is modified by discarding the dissipative part and retaining the non-dissipative part (so-called the gyro-viscous tensor or the gyro-viscosity), which is added to the two-fluid MHD equations while electron inertia is neglected.

The Hall term and the gyro-viscosity have been in-

author's e-mail: goto.ryosuke@nifs.ac.jp

introduced in some nonlinear simulation codes, such as the M3D [11] and the NIMROD code [12]. Our nonlinear simulation code, the MHD In the Non-Orthogonal System (MINOS) [5], has also been used to study the Hall effects on the growth of the ballooning modes in the LHD [13]. However, a large computational resource is often required to study the effects of the extension of the MHD equations since many aspects of the effects appear in the short-length-scales, and it is not very effective to study the effects of the extension over a wide range of the parameter space of a toroidal plasma by using full 3D nonlinear code. Thus, in this paper, we restrict ourselves in this paper to a simplified problem; the Rayleigh-Taylor (R-T) instability in a 2D slab. Though a 3D nature is discarded in the simplified problem, a sufficient numerical resolution to study the effects of the extension of the MHD equations becomes affordable by the simplification.

In this paper, we further restrict ourselves to an inviscid problem in order to see the influence of the Hall and the FLR terms on the short-length-scale mode clearly.

The R-T instability in a 2D slab has been studied both theoretically and numerically [14–18]. Roberts and Taylor [14] have introduced the FLR effect as the anisotropic pressure, which is called now as the gyro-viscous tensor, and have shown the dispersion relation for an idealized equilibrium.

Huba [15] has carried out 2D MHD simulations with the FLR effect (the equations are referred to as *FLR MHD equations*) and has shown the stabilization of the short-wave-length modes and difficulty of the stabilization of the long-wave-length modes. Winske [16] has carried out 2D hybrid simulation, and has shown that the gyro-viscous term stabilizes the short-length-scale modes while the Hall term destabilizes them. Huba and Winske [17] have carried out both 2D extended MHD simulations and hybrid simulations, and have shown that the short-length-scale modes in the hybrid simulations are highly stabilized compared with the single-fluid MHD simulations.

Zhu *et al.* [18] have reported their numerical results of extended MHD simulations for the linear stage of time evolution. Although these studies have revealed some aspects of the two-fluid effects and the FLR effects, there still remain some important aspects to be clarified. For example, typical parameters such as the β -value and the density ratio are sometimes suitable for the space plasma parameters and can be different from those in fusion plasma. Simulations for extended MHD simulation with low density ratio and low β values can provide some advances in our knowledge on the extended MHD effects. Furthermore, extended effects in the nonlinear stage of the R-T instability are not clarified yet.

In this paper, the growth of the R-T modes in a rectangular slab is studied numerically by means of the extended MHD simulations. This paper is organized as follows. In §2, the outline of our simulations is shown. In §3, numerical results are shown. In §3.1, the linear stage of the

instability in our simulations is characterized by the linear growth rates. In §3.2, some nonlinear aspects in the time evolution of the R-T modes are studied. Summary is shown in §4.

2. System of Equations and Initial Equilibrium

The Braginskii-type MHD equations that include the Hall term and the gyro-viscosity, or the extended MHD equations, in a 2D rectangular slab can be expressed as

$$\frac{\partial \rho}{\partial t} = -\nabla \cdot (\rho \mathbf{v}), \quad (1)$$

$$\frac{\partial}{\partial t} (\rho \mathbf{v}) = -\nabla \cdot \left[\rho \mathbf{v} \mathbf{v} + \mathbf{I} \left(p + \frac{B^2}{2} \right) - \mathbf{B} \mathbf{B} + \delta \mathbf{\Pi}^{gv} \right] + \rho \mathbf{g}, \quad (2)$$

$$\frac{\partial E_t}{\partial t} = -\nabla \cdot [(E_t + p) \mathbf{v} + \mathbf{v} \cdot \delta \mathbf{\Pi}^{gv}] + \mathbf{v} \cdot \mathbf{J} \times \mathbf{B} + \rho \mathbf{g} \cdot \mathbf{v}, \quad (3)$$

$$\frac{\partial \mathbf{B}}{\partial t} = -\nabla \cdot (\mathbf{v} \mathbf{B} - \mathbf{B} \mathbf{v}) - \nabla \times \left[\frac{\epsilon}{\rho} (\mathbf{J} \times \mathbf{B} - \nabla p_e) \right], \quad (4)$$

where the total energy E_t is defined as $E_t \equiv p/(\gamma - 1) + \rho v^2/2$, and $\gamma = 5/3$ is the ratio of specific heats. The total pressure is defined as $p = p_i + p_e = (\alpha + 1)p_e$, $\alpha = p_i/p_e$ where p_i and p_e are the ion and the electron pressures, respectively. The system is assumed to be uniform in the third direction, $\partial/\partial z = 0$ and the two-dimensional velocity field vector $\mathbf{v} = (u, v, 0)$ in Eqs.(1)-(4), while keeping the third component of the magnetic field vector $\mathbf{B} = (B_x, B_y, B_z)$. The gyro-viscosity is given by

$$\Pi^{gv}_{xx} = -\Pi^{gv}_{yy} = -p_i \left(\frac{\partial v}{\partial x} + \frac{\partial u}{\partial y} \right), \quad (5)$$

$$\Pi^{gv}_{xy} = \Pi^{gv}_{yx} = p_i \left(\frac{\partial u}{\partial x} - \frac{\partial v}{\partial y} \right). \quad (6)$$

The last term on the right-hand-side of Eq. (4) consists of the Hall term and the electron pressure gradient, which represents two-fluid effects. All variables in Eqs.(1)-(4) have already been normalized by representative quantities: the scale length L , the characteristic values of the background magnetic field B_0 which is in the z direction and the mass density $\rho_0 = mn_0$, the Alfvén velocity $V_A = \sqrt{B_0^2/(\mu_0 \rho_0)}$ where μ_0 is the vacuum permeability, the Alfvén time scale L/V_A , B_0^2/μ_0 for the pressure, and V_A^2/L for the gravitational acceleration $\mathbf{g} = (0, -g, 0)$. The symbols δ and ϵ represent the coefficients of the gyro-viscosity and the Hall term, respectively. The two coefficients are related to each other as $\epsilon = 2B_Z \delta = d_i/L$ where $d_i = \sqrt{m/(\mu_0 n_0 e^2)}$ is the ion skin depth, e is the electric charge, and B_Z is the strength of the normalized magnetic field in the equilibrium in our normalization. However, the Hall term and the gyro-viscosity term are often adopted independently in

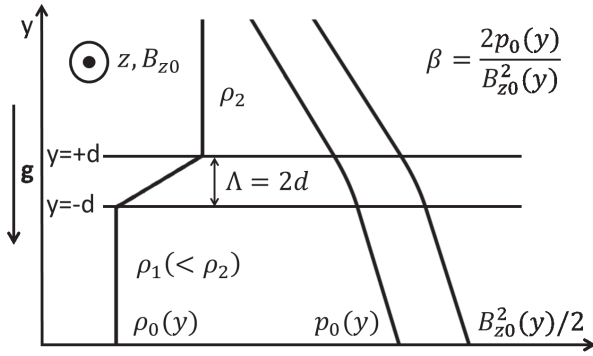


Fig. 1 Schematic view of the initial equilibrium for the R-T instability study. The profiles of ρ , p_0 and $B_{z0}^2/2$ are refracted at $y = \pm d$, in accordance with Eqs. (7) and (8).

some fluid models, dependent to the ordering in the models. In this article, the two parameters are given independently to each other and examine the roles of these terms to study the effect of the adoption/omission of these terms.

For studying the R-T problem, a 2D rectangular region $-\pi \leq x \leq \pi$ and $-3\pi \leq y \leq 3\pi$ is considered. Periodic boundary condition is imposed at $x = \pm\pi$, while the simple outflow condition $\partial/\partial y \rightarrow 0$ are used at $y = \pm 3\pi$. The initial density profile $\rho_0(y)$ is given by connecting the upper region of the density ρ_2 and the lower region of the density ρ_1 by the linear function as

$$\rho_0(y) = \begin{cases} \rho_2 & (y \geq d) \\ \rho_1 + \frac{\rho_2 - \rho_1}{2d}(y + d) & (|y| < d) \\ \rho_1 & (y \leq -d) \end{cases} \quad (7)$$

The initial pressure $p_0(y)$ and the magnetic field $B_{z0}(y)$ satisfy the equilibrium equation

$$\frac{\partial}{\partial y} \left(p_0(y) + \frac{B_{z0}(y)^2}{2} \right) = -\rho_0 g, \quad (8)$$

which is integrated

$$p_0(y) + \frac{B_{z0}(y)^2}{2} = \begin{cases} -\rho_2 g y + \frac{1}{4}(\rho_2 - \rho_1) g d + \frac{B_Z^2}{2} & (y \geq d) \\ -\rho_1 g y - \frac{\rho_2 - \rho_1}{2d} g \left(\frac{y^2}{2} + d y \right) + \frac{B_Z^2}{2} & (|y| < d) \\ -\rho_1 g y + \frac{1}{4}(\rho_2 - \rho_1) g d + \frac{B_Z^2}{2} & (y \leq -d) \end{cases} \quad (9)$$

Here, the integration constants are given by the condition

$$p_0(0) + \frac{B_{z0}^2(0)}{2} = \frac{B_Z^2}{2}. \quad (10)$$

Finally, the initial pressure $p_0(y)$ and the magnetic field $B_{z0}(y)$ are given from Eq. (9) with the beta value $\beta \equiv 2p_0/B_{z0}^2$ kept constant, which is given as the control parameter.

Initial equilibrium is characterized by such parameters

Table 1 Parameter space used in our simulations.

run number	Nx	Ny	β	δ	ϵ	D
1	1024	4096	10.0%	0.00	0.00	2.0
2	1024	4096	10.0%	0.07	0.00	2.0
3	1024	4096	10.0%	0.10	0.00	2.0
4	1024	4096	10.0%	0.00	0.10	2.0
5	1024	4096	10.0%	0.00	0.30	2.0
6	1024	4096	10.0%	0.07	0.10	2.0
7	1024	4096	10.0%	0.10	0.10	2.0
8	1024	4096	10.0%	0.07	0.30	2.0
9	1024	4096	10.0%	0.00	0.00	3.0
10	1024	4096	10.0%	0.10	0.00	3.0
11	1024	4096	10.0%	0.00	0.10	3.0
12	1024	4096	10.0%	0.10	0.10	3.0

as the density ratio $D = \rho_2/\rho_1$, the jump width of the density $\Lambda = 2d$, and the β value, as illustrated in Fig. 1. In order to study the R-T instability, the system of equations (1)-(4) are solved numerically by using the fourth-order central difference scheme and fourth-order Runge-Kutta-Gill method. Since neither the physical viscosity nor the resistivity is added, the fourth-order hyperviscosity is added to the system to suppress a numerical noise. Numerical tests have carried out for various numbers of grid points (N_x, N_y) and for various coefficients of the hyperviscosity to clarify the range of wave numbers affected by the hyperviscosity. In the numerical results in the following sections, we restrict ourselves to the range of wave numbers in which the influence of hyperviscosity can be neglected.

3. Numerical Results

Numerical simulations of some parameters shown in Table 1 are carried out. The ratio between ion and electron pressures $p_i/p_e = 1.0$, $g = 0.1$, $\beta = 10.0\%$, $B_Z = 10.0$, and $\Lambda = 1.0$ is assumed throughout the simulations. In §3.1, the linear stage of the R-T instability which is governed by the extended MHD equations (1)-(4) is seen. In §3.2, some aspects in the nonlinear evolution are discussed.

3.1 Linear stage of the R-T instability

The linear stage of the time evolution of unstable modes can be well studied by Fourier power spectra. The Fourier transform of a variable $A(x, y, t)$ in the x -direction gives the Fourier coefficient $\tilde{A}(k_x, y, t)$ of the wave number k_x . Integration of the Fourier energies in the y -direction, $P_A(k_x, t) = \int |\tilde{A}(k_x, y, t)|^2 dy$ gives the power spectrum of the variable A . Figure 2 shows the time evolution of the kinetic energy spectrum $\frac{1}{2} [P_u(k_x, t) + P_v(k_x, t)]$ in runs (a) 1, (b) 3, (c) 4 and (d) 7. For simplicity, the wave numbers in the figures is limited for $1 \leq k_x \leq 20$, although the exponential growth of the Fourier energies are observed well for larger values of k_x 's. While the growth rates of the Fourier modes of the velocity field in Figs. 2 (a)-(c) are compara-

ble to each other and show only a little dependence on the wave number, Fig. 2(d) shows a clear dependence of the growth rates on the wave numbers. (See the next paragraph on the dependence of the growth rates on the wave number). It may be worth noting on a period of the linear stage in the simulations. In Figs. 2(a)-(c), many of the Fourier modes move to their nonlinear stage after $t \sim 40$ and are saturated at $t \simeq 60$. However, in Fig. 2(d), the linear growth of some Fourier modes continues until $t \simeq 60$ and is saturated only after $t \simeq 70$. It is considered that the difference can be attributed to the reduction of the growth rates of high wave number modes in Fig. 2(d). Because of the reduction, the numbers of Fourier modes which can influence the growth of the low Fourier modes through the nonlinear couplings with sufficient amplitudes are decreased. Consequently, the period of the linear stage in Fig. 2(d) continues longer than in the other three runs.

By fitting an exponential function to the Fourier power spectra, the linear growth rate σ in the simulation can be estimated as a function of the wave number k_x . The growth rates are shown in Fig. 3(a) for $D = 2.0$ and (b) for $D = 3.0$, respectively. The growth rates in Fig. 3(b) look being amplified by a factor of about $3/2$ compared to those in Fig. 3(a). In the single-fluid MHD cases (the run 1 in Fig. 3(a) and the run 9 in Fig. 3(b)), σ increases as a function of the wave number k_x and approaches to the constant value in the large wave number limit. This behavior is consistent with our preliminary results of linear eigenmode analysis of the R-T instability (the detailed results will be shown elsewhere). In runs 2 and 3 in Fig. 3(a) and 10 in Fig. 3(b), the FLR effect on the R-T instability is examined by varying δ and keeping $\epsilon = 0.00$. The results do not show a large change in the growth rates excepting a weak reduction of σ at high wave number region. In runs 4 and 5, the two-fluid effect is examined by varying ϵ while keeping $\delta = 0.00$. The introduction of the two-fluid effect does not bring about a clear difference from the single-fluid MHD case. Even in run 5 with $\epsilon = 0.30$, which is the largest ϵ among our numerical simulations, σ is increased by only a several percent from that of the single-fluid MHD case.

Though the change of the growth rates by the FLR and the two-fluid effects is not very large, the tendency of the decrease/increase of the growth rates are consistent with the earlier results seen in Refs. [14–18]. In those papers, it has been reported that the gyro-viscosity can stabilize unstable modes, whether the stabilization is complete or partial, while the two-fluid term can destabilize the modes. A notable change of the growth rate is found in our simulations when δ and ϵ are set to be non-zero. In run 7 where $\delta = 0.10$ and $\epsilon = 0.10$, the growth rate at relatively high wave number modes are reduced considerably. In fact, the reduction is much larger than that expected from the growth rates in run 3 and 4, where only one of δ or ϵ is set non-zero. While Huba and Winske [17] have reported the growth rates similar to those in runs 7 and 8, they have not reported separate dependence of the growth rates on the

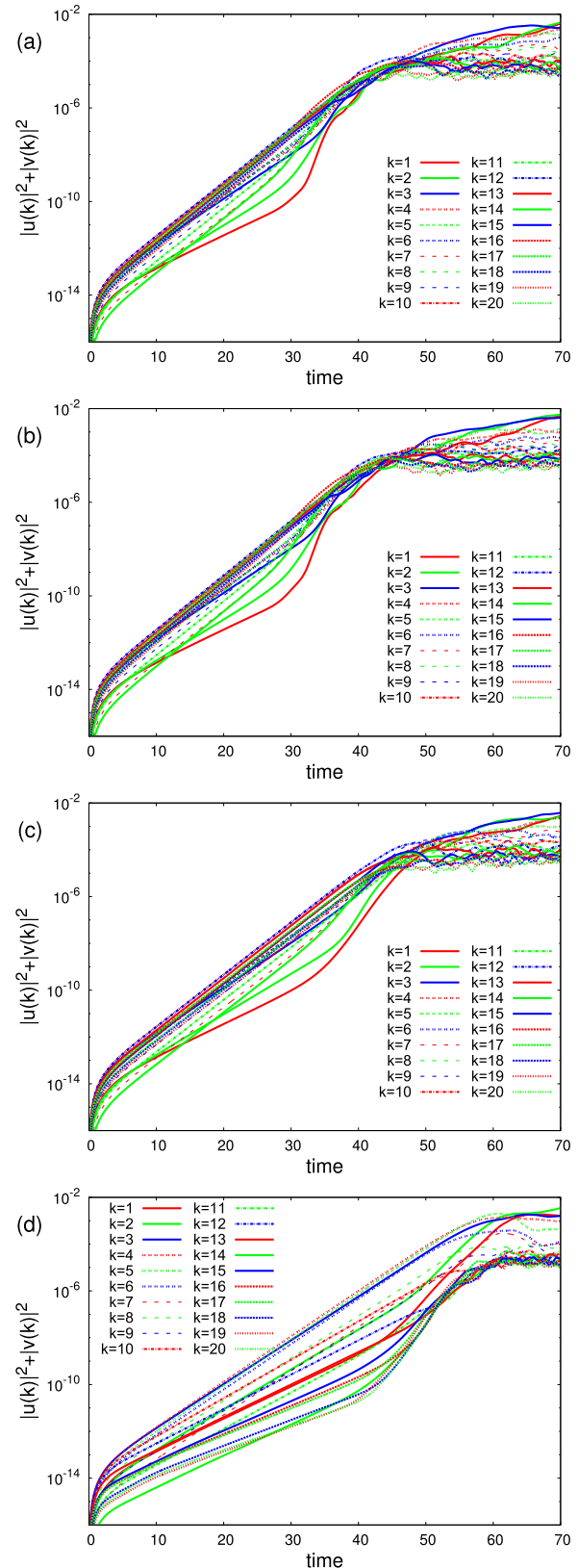


Fig. 2 Time evolution of the integrated kinetic energy in runs (a) 1 ($\epsilon = \delta = 0.00$), (b) 3 ($\epsilon = 0.10, \delta = 0.00$), (c) 4 ($\epsilon = 0.00, \delta = 0.10$) and (d) 7 ($\epsilon = 0.10, \delta = 0.10$). In (a)-(c), many of the Fourier modes move to the nonlinear stage after $t \sim 40$ and are saturated at $t \simeq 60$. However, in (d), the linear growth of some Fourier modes continues until $t \simeq 60$ and is saturated only after $t \simeq 70$.

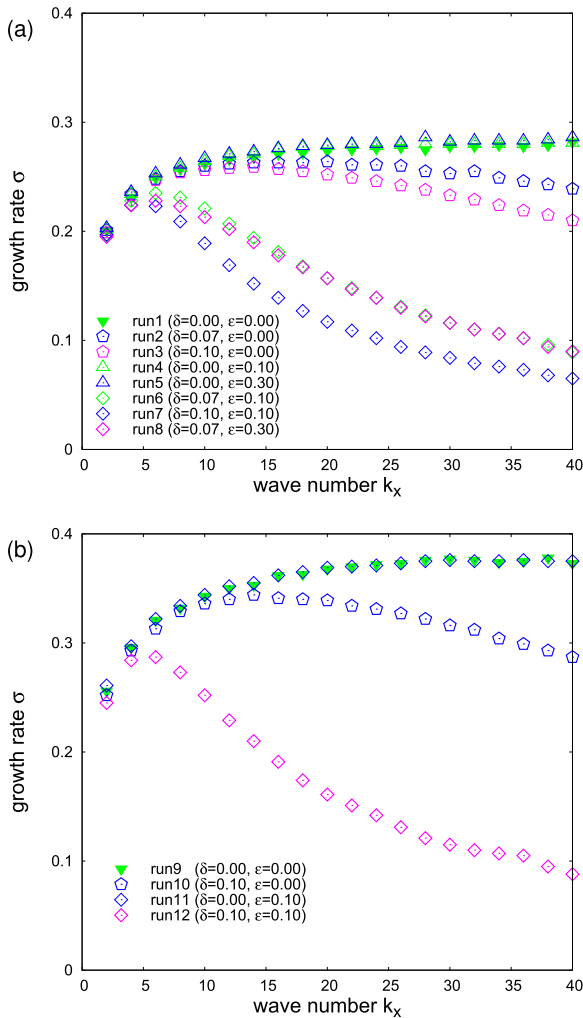


Fig. 3 Linear growth rates obtained by simulations with the density ratio (a) $D = 2.0$ and (b) $D = 3.0$. The growth rates of high wave number modes are strongly decreased when both of δ and ϵ are finite.

Hall term and the gyro-viscosity. It may be partially because the effects of δ and ϵ can not be separated in the hybrid simulations. As Huba and Winske have reported that their hybrid simulations agree well with fluid simulations (for finite δ and ϵ) [17], it is expected that our growth rates will also agree if we carry out hybrid simulations. Our numerical results show that the reduction of the growth rates is provided by the coupled effect of the gyro-viscosity and the two-fluid term. The observation suggests that, in comparison to models which include either the two-fluid term or the gyro-viscosity, a model with both of them can show a considerable reduction of the growth rates. In other words, the truncation of the two-fluid term in some assumptions can weaken the FLR effect to suppress the growth of the R-T instability.

3.2 Some aspects of nonlinear evolution

One convenient measure of the impact of the instability on initial equilibrium is the saturation level of the

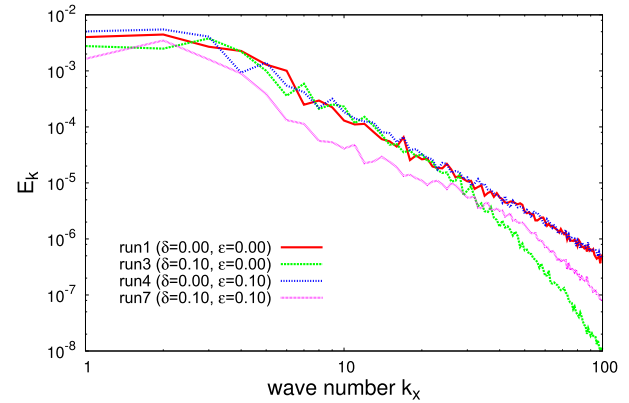


Fig. 4 Energy spectrum of the velocity field at $t = 70$. Energy of the low wave number modes ($k_x \leq 30$) are reduced in run7.

growth of unstable modes. In Fig. 4, the velocity energy spectrum at $t = 70$ is shown. (See also Fig. 2 again for the time evolution of the energy spectra). The wave number range is restricted to $k_x \leq 100$ since the observation of the spectrum at high wave numbers is meaningless because the high wave number range is artificially suppressed by the hyperviscosity.

The energy of Fourier modes in run 7 is smaller than those in runs 1 and 4 for all wave number region in this figure. In addition, the Fourier energy in run 7 is smaller than those in run 3 for $k_x \leq 30$, but it is larger for $k_x \geq 30$.

These differences between the two spectra are attributed to the value of the Hall coefficient ($\epsilon = 0.00$ and 0.10 in the runs 3 and 7, respectively). It may be that in run 7, the two-fluid term can raise the energy in the high wave number region while it can reduce the energy in the low wave number region, although we can not assert it now.

For the purpose of characterizing the impact of the instability in the nonlinear process, we introduce the mixing width. The mixing width at each horizontal coordinate x is defined as the distance between two points, the maximum y where the mass density becomes smaller than the heavier mass density ρ_2 by 1%, that is $\max[y(0.99\rho_2)]$, and the minimum y where the mass density becomes larger than the lighter mass density ρ_1 by 1%, that is $\min[y(1.01\rho_1)]$. Here, the distance between two points in the y -direction is defined as the local mixing width. In Fig. 5 (a), the density contours of $t = 50$ in run 1 (the $D = 2.0$ runs) are shown, together with two thick black lines, which give the two levels $\rho = 0.99\rho_2$ and $\rho = 1.01\rho_1$. The local mixing width is the distance between the two black lines in the y -direction. Then the mixing width is given as the averaged value of the local mixing width,

$$d_{\text{mix},x_i} \equiv \frac{1}{2\pi} \int \{ \max[y(0.99\rho_2)]|_x - \min[y(1.01\rho_1)]|_x \} dx. \quad (11)$$

From the definition, the initial value of the mixing width

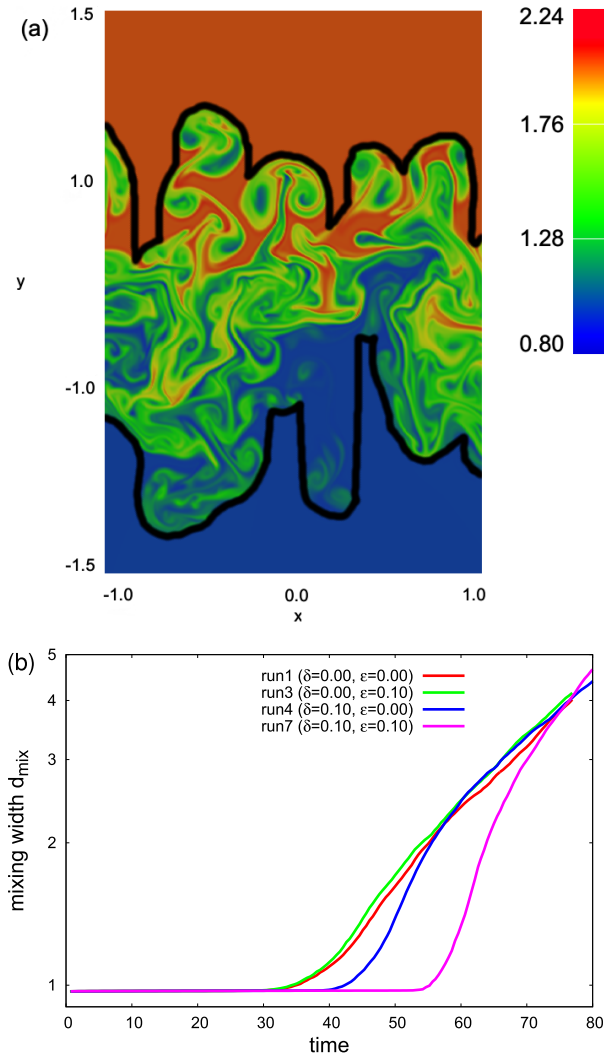


Fig. 5 (a) Contours of the mass density at $t = 50$ in run 1 for $-1 \leq x \leq 1$ and $-\pi/2 \leq y \leq \pi/2$, drawn together with the two black lines, distance of which in the vertical line gives the mixing width. (b) Time evolution of mixing width for the density ratio for $D = 2.0$. While the mixing width in runs 1 and 3 begin to grow earlier than the others, the mixing width of runs 4 and 7 catch up by $t = 70$.

d_{mix} is almost the same as the jump width Λ . The mixing width d_{mix} gives an obvious growth of the mixing (turbulent) region in the nonlinear stage of the time evolution. Similar characterization is often found in R-T turbulence studies. (See Ref. [19], for example). In Fig. 5 (b), the time evolution of the mixing width in the four $D = 2.0$ runs (runs 1, 3, 4, and 7) are shown.

While the mixing width in the runs 1 and 3 begin to grow earlier than that in the others, the mixing width of runs 4 and 7 catch up by $t = 70$.

The growth of the mixing width is not saturated even though the growth of the unstable modes in these runs are saturated by $t = 70$ as seen in Fig. 2. It is another expression of the simple fact that the growth of the displacement is not saturated even though the growth of the velocity is

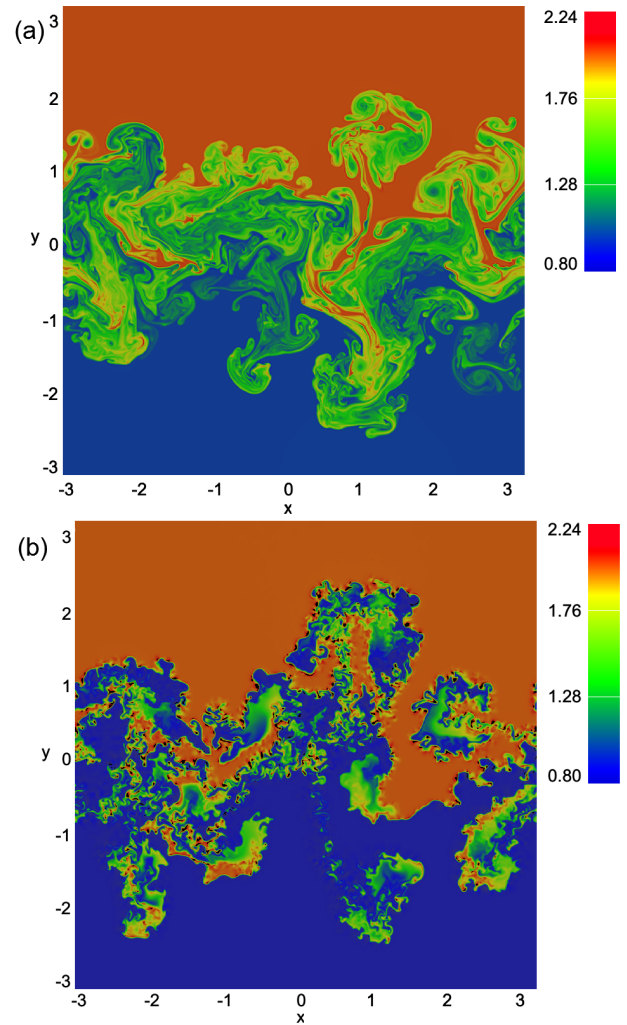


Fig. 6 Contour plots of the mass density ρ at $t = 70$ in runs (a) 1 ($\delta = \epsilon = 0.00$) and (b) 7 ($\delta = 0.10, \epsilon = 0.10$). The region of $-\pi \leq x \leq \pi$ and $-\pi \leq y \leq \pi$ is shown. In (a), the two contour lines $\rho = \rho_2$ and $\rho = \rho_1$ are relatively separated and the density contours change smoothly between them. In (b), the distance between the two contour lines, being drawn as the mixture of the red ($\rho = \rho_2$) and blue ($\rho = \rho_1$) regions, are much narrower than that in (a) meaning that there is a sharp density gradient in (b).

saturated. In order for the growth of the mixing width to be saturated, the Fourier energies of the velocity must be damped quickly.

In Fig. 6, the contour plots of the mass density ρ at $t = 70$ are shown. Figure 6 (a) is for run 1, which is the single-fluid MHD case. Due to this simultaneous growth of the R-T modes, many mushroom-like structures are formed in the mixing or turbulent region. Figure 6 (b) is for run 7, where two-fluid and FLR effects are included simultaneously. Here, two runs 1 and 7, are compared, and other runs, such as runs 3 and 4, are omitted because their mass density contours are qualitatively similar to those in Fig. 6 (a).

The density contour plots in Fig. 6 (b) look more com-

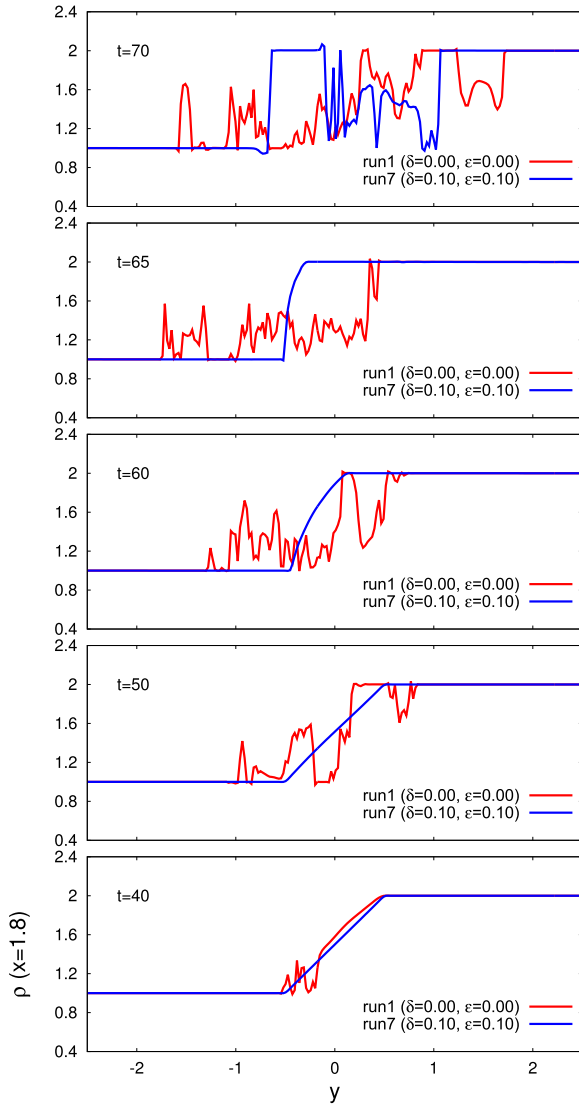


Fig. 7 Mass density ρ from $t = 40$ to $t = 70$ in runs 1 and 7. From lower to upper, the panels are for $t = 40, 50, 60, 65$ and 70 . While the density plot of run 1 (red) shows strong variations, the density of run 7 (blue) changes quite slowly in comparison to that of run 1.

plicated than those observed by Huba and Winske [17], in which the fine structures are called as the *bubbles and spikes*. Though there are many bubbles and spikes in Ref. [17], each of them look smoother than the fine structures in our simulation. The difference may be attributed to the difference of the numerical resolution because the number of the grid points in Ref. [17] is typically (100, 256), while in our simulations it is (1024, 4096).

In Figs. 6 (a) and (b), some differences are observed, especially in the fine structures of the contours. In Fig. 6 (a), the contour lines of $\rho = \rho_2$ and $\rho = \rho_1$ consist of relatively smooth lines, which can be recognized as the simple consequence of the growth of mushroom-like structures associated with the R-T instability. Furthermore, the two contour lines $\rho = \rho_2$ and $\rho = \rho_1$ are relatively sepa-

rated and the density contours change smoothly between them. In contrast, in Fig. 6 (b), the distance between two contour lines, being drawn as a mixture of red ($\rho = \rho_2$) and blue ($\rho = \rho_1$), are much narrower than that in Fig. 6 (a). It means that there is a sharp density gradient in Fig. 6 (b). Such a difference between Figs. 6 (a) and (b) can be seen more clearly by plotting the density along the coordinate line.

In Fig. 7, densities in the runs 1 and 7 are plotted along the y -coordinate line for $t = 40, 50, 60, 65$ and 70 . While the density plot of run 1 shows strong variations, the density of run 7 changes quite slowly in comparison to that of run 1. At the final time $t = 70$, it is obviously observed that the density in run 7 falls sharply from $\rho = \rho_2$ to $\rho = \rho_1$, while that in run 1 shows sharp oscillations between the two levels $\rho = \rho_1$ and $\rho = \rho_2$. It indicates a tendency that strong density fluctuations are removed by the effects of the gyro-viscosity and the Hall term, and the stabilization effects influence even in the nonlinear stage. However, we have not clarified the reason behind the occasional fall of density from $\rho = \rho_2$ to ρ_1 so sharply. A detailed analysis of the mechanism, as well as behaviors of other variables, will be presented in our forthcoming paper with finer numerical resolutions.

4. Summary

The effects of the two-fluid term and the gyro-viscosity are studied by the nonlinear extended MHD simulations.

The numerical simulations have been carried out by changing the coefficients of the two-fluid and the gyro-viscosity terms independently to each other for a parameter region which is closer to that of a torus plasma.

Introduction of the Hall term slightly increases the linear growth rate over entire range of wave numbers, while the gyro-viscosity reduces the growth rates of modes having relatively high wave number. Inclusion of both terms causes larger reduction of the growth rates than that expected from the growth rates in the other simulations.

Our numerical results show that the truncation of the two-fluid term in some orderings can weaken the FLR effect that suppresses the growth of the R-T instability.

The impact of the reduction of the growth rates at high wave numbers on low wave number modes are studied by using the mixing width. Although the growth of the mixing width is slowed down by combining the Hall term and the gyro-viscosity, the mixing width finally reaches the same level in all runs. However, the density profile in runs with the Hall term and the gyro-viscosity, is quite sharper than that in the single-fluid MHD run, suggesting a smoothing effect of the gyro-viscosity.

In this paper, we have restricted ourselves 2D simulations. However, 3D natures can play important roles in a torus plasma. Full 3D simulations will be presented in our forthcoming paper.

Acknowledgments

This work was partly supported by KAKENHI 23540583 and 24740375.

- [1] A. Komori *et al.*, *Fusion Sci. Technol.* **58**, 1 (2010).
- [2] H. Zohm, *Plasma Phys. Control. Fusion* **38**, 105 (1996).
- [3] P.B. Snyder *et al.*, *Phys. Plasmas* **9**, 2037 (2002).
- [4] K. Ichiguchi, N. Nakajima, M. Wakatani, B.A. Carreras and V.E. Lynch, *Nucl. Fusion* **43**, 1101 (2003).
- [5] H. Miura and N. Nakajima, *Fusion Sci. Technol.* **51**, 8 (2007).
- [6] K. Ichiguchi and B. Carreras, *Nucl. Fusion* **51**, 053021 (2011).
- [7] H. Miura and N. Nakajima, *Nucl. Fusion* **50**, 054006 (2010).
- [8] S. Sakakibara *et al.*, *Plasma Fusion Res.* **1**, 003 (2006).
- [9] S.I. Braginskii, in *Reviews of plasma physics*, edited by M.A. Leontovich (Consultants Bureau, New York, 1965) **1**, p. 205.
- [10] D.D. Schnack *et al.*, *Phys. Plasmas* **13**, 058103 (2006).
- [11] W. Park *et al.*, *Phys. Plasmas* **6**, 1796 (1999).
- [12] C.R. Sovinec *et al.*, *J. Comput. Phys.* **195**, 355 (2004).
- [13] H. Miura and N. Nakajima, the 23rd IAEA fusion energy conference (Daejon, Korea, Oct.11-16, 2010) TH-P9/16.
- [14] K.V. Roberts and J.B. Taylor, *Phys. Rev. Lett.* **8**, 197 (1962).
- [15] J.D. Huba, *Phys. Plasmas* **3**, 2523 (1996).
- [16] D. Winske, *Phys. Plasmas* **3**, 11 (1996).
- [17] J.D. Huba and D. Winske, *Phys. Plasmas* **5**, 2305 (1998).
- [18] P. Zhu *et al.*, *Phys. Rev. Lett.* **101**, 085005 (2008).
- [19] N. Vladimirova and M. Chertkov, *Phys. Fluids* **21**, 015102 (2009).